

Topology-dependent criticality in triplet majority-rule dynamics with collective reversal on quenched networks

Roni Muslim

*Asia Pacific Center for Theoretical Physics
Pohang 37673, Republic of Korea
Research Center for Quantum Physics, BRIN,
South Tangerang, 15314, Indonesia
roni.muslim@apctp.org*

We study a triplet majority-rule opinion-dynamics model with collective reversal on quenched networks. Interactions occur on local triplets composed of one agent and two of its neighbors, while collective reversal acts only on unanimous triplets. This rule separates local conformity from external perturbations that disrupt local agreement. We show that quenched network topology shifts the order–disorder critical point away from the well-mixed value. For Barabási–Albert, Erdős–Rényi, and random regular networks, the critical point is shifted while the critical exponents remain close to the mean-field values. By contrast, Watts–Strogatz networks exhibit a much lower critical point and stronger deviations in the effective critical exponents, highlighting the role of clustering and local correlations. A rewiring analysis of Watts–Strogatz networks further shows that the ordered phase becomes more stable as the network becomes more random. These results indicate that quenched topology not only sets the transition point, but also leads to topology-dependent effective critical behavior in networks with strong clustering and local correlations.

Keywords: Opinion dynamics; majority-rule model; quenched networks; collective reversal; finite-size scaling.

PACS Nos.: 89.65.-s, 89.75.Hc, 05.70.Fh, 05.10.Ln, 64.60.aq

1. Introduction

Opinion dynamics is an important topic in sociophysics because it provides a minimal framework for understanding how local interactions among individuals can generate collective behavior at the population level. In agent-based approaches, individuals are usually represented by discrete opinion variables, while opinion changes are governed by microscopic update rules. Despite their simplicity, such models can reproduce various macroscopic phenomena, such as consensus, coexistence, polarization, and order–disorder transitions.^{1–9} Binary-opinion models, with $s_i = +1$ or $s_i = -1$, provide a useful starting point for describing competition between two opposing social choices, such as support and opposition, adoption and resistance, or trust and distrust.

One of the basic mechanisms in opinion formation is local conformity. In majority-rule dynamics, a small group of agents interacts and the majority opinion

2 *R. Muslim*

within the group determines the direction of the update. This mechanism differs from the voter model, which is based on imitation of a single neighbor, because the update is determined by the opinion composition of a local group.^{10–15} Thus, majority-rule dynamics can be viewed as a minimal representation of small group discussions, local social pressure, or the tendency of individuals to follow the dominant view in their social environment.

Most analytical formulations of majority-rule and related opinion models have been developed in the well-mixed or annealed setting, where interaction groups are randomly selected from the entire population. This approach is analytically convenient because group statistics can be written as functions of the global opinion density. However, real social interactions usually take place on relatively fixed contact structures, such as friendship networks, communities, organizations, or online platforms. Therefore, opinion dynamics on quenched networks is important for understanding how degree heterogeneity, hubs, clustering, and local correlations affect collective opinion formation.^{16–23} This is particularly relevant in capturing the empirical characteristics of digital echo chambers, where fixed social structures play a critical role in information segregation.²⁴

In addition to local-neighbor influence, opinions may also be affected by external sources, such as media, campaigns, institutional messages, or macroscopic social pressure. In many models, such effects are introduced as external fields, noise, independence, anticonformity, zealotry, or stubbornness.^{14, 25–31} In this study, we model external influence in a different way, namely as collective reversal that acts only on local triplets that have reached a unanimous state. Thus, the external perturbation does not act on all local configurations, but selectively reverses small groups that have already formed local agreement.

Specifically, we study triplet majority-rule dynamics on quenched networks. In each elementary update, a central node r is selected at random, and two of its neighbors $j, \ell \in \partial r$ are selected to form a local triplet $\tau = (r, j, \ell)$. Mixed triplets are updated according to the majority rule, whereas unanimous triplets may undergo collective reversal. The formulation on quenched networks introduces challenges that do not arise in well-mixed populations. In the well-mixed case, the probability of obtaining a triplet with a given number of positive spins follows a binomial form that depends only on the global density c . In contrast, on quenched networks, two configurations with the same value of c may have different local arrangements. As a result, triplet frequencies are no longer determined by c alone, but also by the network structure and the local correlations generated during the dynamics. This makes a homogeneous mean-field approximation insufficient for capturing the influence of topology on the critical point and collective behavior.

To address this issue, we construct a projected master-equation description in the aggregate variable q , defined as the number of agents holding opinion $+1$. Network information is retained through the conditional local-triplet statistics $R_a(q; \epsilon)$, where $a = 0, 1, 2, 3$ denotes the number of positive spins in the selected triplet. In contrast to the binomial mean-field approximation, the transition rates in this

description are determined by the actual triplet statistics on quenched networks. Methodologically, $R_a(q; \epsilon)$ is interpreted as a local statistic obtained from stationary microscopic configurations, rather than as a direct fit to the order-parameter curve. The approach is validated by comparing Monte Carlo (MC) simulations, the full master equation for small systems, and the projected master equation.

The main contributions of this article are threefold. First, we study a triplet majority-rule model on quenched networks with collective reversal on unanimous triplets. Second, we show that the projected master equation based on $R_a(q; \epsilon)$ can reproduce the aggregate dynamics obtained from MC simulations and, for small systems, from the full master equation. Third, we analyze the order–disorder transition on several network topologies, namely Barabási–Albert (BA), Erdős–Rényi (ER), random regular (RR), and Watts–Strogatz (WS) networks, using finite-size scaling.^{22, 23, 32–35} Our results show that the quenched network structure not only shifts the critical point away from the well-mixed value, but also leads to topology-dependent effective critical behavior, particularly when local correlations and clustering are strong.

This study is also related to recent developments in opinion dynamics based on group interactions and higher-order interactions. Although the interaction substrate in our model is a pairwise network, the update rule acts collectively on local triplets. In this sense, the present model captures a higher-order-like update mechanism without introducing explicit hyperedges.^{36–41} Thus, the model provides a minimal framework for connecting local update rules, triplet statistics on fixed networks, and macroscopic critical behavior.

2. Model Description

We consider an opinion-dynamics model based on majority rule on a quenched network. The system consists of N agents located on the nodes of an undirected network with adjacency matrix A_{ij} . Each agent i carries a binary opinion $s_i = \pm 1$, where $s_i = +1$ and $s_i = -1$ represent two competing opinions. The network structure is kept fixed throughout the dynamics, so interactions do not occur randomly over the whole population, but are constrained by the existing neighbor relations.

The degree of node i is defined as $k_i = \sum_{j=1}^N A_{ij}$, and its set of neighbors is denoted by ∂i . At each elementary update, a central node r is selected at random. Since the update requires two neighbors, only nodes with $k_r \geq 2$ can serve as the center of a triplet. If the selected node has $k_r < 2$, the central node is redrawn until an eligible node is obtained. Once the central node r is chosen, two distinct neighbors $j, \ell \in \partial r$ are selected uniformly at random without replacement. Thus, the interaction group always has size three, $n = 3$, and the updated local triplet is $\tau = (r, j, \ell)$.

The update rule consists of two mechanisms. The first mechanism is local conformity through majority rule. If two of the three agents in the triplet hold opinion $+1$, then all members of the triplet adopt opinion $+1$, namely $++- \rightarrow +++$.

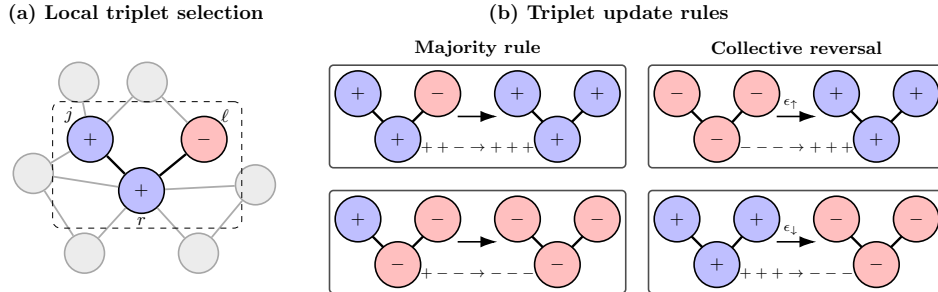
4 *R. Muslim*


Fig. 1. Illustration of the local triplet update on a quenched network. (a) A central node r is selected at random from nodes that can form a triplet, and two distinct neighbors j and ℓ are then selected to form the triplet $\tau = (r, j, \ell)$. (b) The triplet is updated either by majority rule, $++- \rightarrow +++$ and $+-- \rightarrow ---$, or by collective reversal in a unanimous state, $--- \rightarrow +++$ with probability ϵ_{\uparrow} and $+++ \rightarrow ---$ with probability ϵ_{\downarrow} .

Conversely, if two of the three agents hold opinion -1 , then all members of the triplet adopt opinion -1 , namely $+-- \rightarrow ---$. Since the group size is always odd, no tie occurs in the majority update.

The second mechanism is collective reversal in the fully unanimous state. In a unanimous state, majority rule produces no change because all members of the triplet already hold the same opinion. However, an external influence can reverse the opinion of the entire triplet collectively. Specifically, the transition $--- \rightarrow +++$ occurs with probability ϵ_{\uparrow} , whereas the transition $+++ \rightarrow ---$ occurs with probability ϵ_{\downarrow} , with $0 \leq \epsilon_{\uparrow}, \epsilon_{\downarrow} \leq 1$. If no reversal occurs, the triplet remains in its original unanimous state. The parameter ϵ_{\uparrow} represents an external tendency that drives opinion -1 toward $+1$, while ϵ_{\downarrow} represents an external tendency that drives opinion $+1$ toward -1 .

In the symmetric collective-reversal case, $\epsilon_{\uparrow} = \epsilon_{\downarrow} = \epsilon$, the two opinions are subject to the same level of external perturbation. In contrast, when $\epsilon_{\uparrow} \neq \epsilon_{\downarrow}$, the external perturbation is asymmetric and favors one of the two opinions. The local triplet-selection and update mechanisms are illustrated in Fig. 1.

This model differs from well-mixed or annealed formulations. In the well-mixed setting, interaction groups are randomly selected from the whole population at each update, so each agent can effectively interact with any other agent. In contrast, on a quenched network, interactions are constrained by fixed local connections. Therefore, the opinion dynamics is determined not only by the global opinion fraction, but also by the network topology, degree heterogeneity, hubs, clustering, and local correlations generated during the update process.

From a social perspective, a local triplet can be interpreted as a small interaction unit, such as a discussion between an individual and two of their nearest social contacts. Majority rule represents the tendency of individuals to adjust their opinions to the local pressure of their small group. Collective reversal in the unanimous state represents an external perturbation or information source outside the local

neighborhood, such as media, campaigns, or macroscopic social pressure, that can change the opinion of a group even after it has reached local agreement. Thus, the model captures the competition between local conformity on a fixed social network and external perturbations that can disrupt local consensus, a dynamic that has been observed empirically across various social media platforms.²⁴

3. Results and Discussion

Before analyzing the critical behavior on large networks, we first construct an aggregate description based on the master equation. The purpose is to validate that the macroscopic dynamics observed in MC simulations can be reproduced by a reduced master-equation description that preserves local triplet statistics on quenched networks. After this validation, we analyze the order parameter, susceptibility, Binder cumulant, and finite-size scaling behavior for different network topologies.

3.1. Master-equation formulation and aggregate description

The stochastic dynamics of the model can be described by a master equation in the full configuration space. Let $\mathbf{s} = (s_1, s_2, \dots, s_N)$ denote a microscopic configuration of the system, with $s_i = \pm 1$, and let $P(\mathbf{s}, t)$ be the probability that the system is in configuration \mathbf{s} at time t . The full master equation is given by

$$\frac{dP(\mathbf{s}, t)}{dt} = \sum_{\mathbf{s}'} [W(\mathbf{s}' \rightarrow \mathbf{s})P(\mathbf{s}', t) - W(\mathbf{s} \rightarrow \mathbf{s}')P(\mathbf{s}, t)], \quad (1)$$

where $W(\mathbf{s} \rightarrow \mathbf{s}')$ denotes the transition rate from configuration \mathbf{s} to configuration \mathbf{s}' . This equation expresses the balance between the probability current entering configuration \mathbf{s} and the probability current leaving it. Since transitions occur only through local triplet updates, the explicit form of $W(\mathbf{s} \rightarrow \mathbf{s}')$ is fully determined by the microscopic rule defined in Sec. 2.

For a local triplet $\tau = (r, j, \ell)$, node r is the central node, while $j, \ell \in \partial r$ are two randomly selected neighbors. Since only nodes with $k_r \geq 2$ can form a triplet, we define $\mathcal{V}_2 = \{r \mid k_r \geq 2\}$ and $N_2 = |\mathcal{V}_2|$. In the simulations, if the selected central node has $k_r < 2$, the selection is repeated until a node in \mathcal{V}_2 is obtained. Therefore, the selection weight of a triplet is $\omega_\tau = 1/[N_2 \binom{k_r}{2}]$ for $r \in \mathcal{V}_2$.

The number of positive spins in the triplet $\tau = (r, j, \ell)$ is written as $a_{rj\ell}(\mathbf{s}) = (1 + s_r)/2 + (1 + s_j)/2 + (1 + s_\ell)/2$, with $a_{rj\ell} = 0, 1, 2, 3$. The values $a = 0, 1, 2, 3$ correspond respectively to the triplet configurations $---$, $+-$, $++$, and $+++$. The weighted fraction of local triplets with a positive spins in configuration \mathbf{s} is then given by

$$\Omega_a(\mathbf{s}) = \frac{1}{N_2} \sum_{r \in \mathcal{V}_2} \frac{1}{\binom{k_r}{2}} \sum_{\substack{j, \ell \in \partial r \\ j < \ell}} \mathbf{1}[a_{rj\ell}(\mathbf{s}) = a], \quad a = 0, 1, 2, 3. \quad (2)$$

With this definition, $\sum_{a=0}^3 \Omega_a(\mathbf{s}) = 1$. The quantity $\Omega_a(\mathbf{s})$ can be interpreted as the probability that a local triplet selected according to the dynamical rule contains a

6 *R. Muslim*

positive spins. Thus, $\Omega_a(\mathbf{s})$ connects the microscopic configuration \mathbf{s} to the actual frequency of local triplets on the quenched network. For networks in which all nodes satisfy $k_r \geq 2$, such as the BA, RR, and WS networks used here, one has $N_2 = N$.

Let $q(\mathbf{s}) = \sum_i (1 + s_i)/2$ denote the number of positive spins. In one elementary update, q can change through four channels: $--- \rightarrow +++$ gives $\Delta q = +3$ with probability ϵ_\uparrow , $++- \rightarrow +++$ gives $\Delta q = +1$, $+- - \rightarrow ---$ gives $\Delta q = -1$, and $+++ \rightarrow ---$ gives $\Delta q = -3$ with probability ϵ_\downarrow . Therefore, for a given configuration \mathbf{s} , the transition rates of these channels are $W(q \rightarrow q+3|\mathbf{s}) = \epsilon_\uparrow \Omega_0(\mathbf{s})$, $W(q \rightarrow q+1|\mathbf{s}) = \Omega_2(\mathbf{s})$, $W(q \rightarrow q-1|\mathbf{s}) = \Omega_1(\mathbf{s})$, and $W(q \rightarrow q-3|\mathbf{s}) = \epsilon_\downarrow \Omega_3(\mathbf{s})$. The mean change of q in configuration \mathbf{s} is then

$$\langle \Delta q \rangle_{\mathbf{s}} = 3\epsilon_\uparrow \Omega_0(\mathbf{s}) + \Omega_2(\mathbf{s}) - \Omega_1(\mathbf{s}) - 3\epsilon_\downarrow \Omega_3(\mathbf{s}). \quad (3)$$

The sign of $\langle \Delta q \rangle_{\mathbf{s}}$ indicates the local tendency of the dynamics in configuration \mathbf{s} . The term $\Omega_2 - \Omega_1$ represents the contribution of majority rule, while $3\epsilon_\uparrow \Omega_0 - 3\epsilon_\downarrow \Omega_3$ represents the contribution of collective reversal in unanimous triplets.

Equation (1) is an exact description, but it involves 2^N configurations and is therefore directly solvable only for small systems. In a well-mixed population, triplet statistics can be written as functions of the global density c , allowing the macroscopic dynamics to be obtained in closed form. In contrast, on quenched networks, two configurations with the same value of c or q may have different local arrangements. Consequently, local triplet frequencies are not determined by the global variable alone, but also by the network topology and by local correlations generated during the dynamics.

To build an aggregate description, the dynamics is projected onto the variable $q = 0, 1, \dots, N$, with $c = q/N$ and $m = 2q/N - 1$. This projection reduces the state space from 2^N microscopic configurations to $N + 1$ aggregate states. However, because the variable q alone does not close the dynamics on quenched networks, we introduce the conditional triplet statistics

$$R_a(q; \epsilon) = \langle \Omega_a(\mathbf{s}) | q(\mathbf{s}) = q \rangle_{st, \epsilon}, \quad a = 0, 1, 2, 3. \quad (4)$$

Here, $\langle \dots \rangle_{st, \epsilon}$ denotes an average over stationary configurations at a given value of the collective reversal probability ϵ and over quenched network realizations. In other words, $R_a(q; \epsilon)$ is the average of $\Omega_a(\mathbf{s})$ over all stationary configurations with the same number of positive spins. Since this average is performed on quenched networks, $R_a(q; \epsilon)$ retains information about degree heterogeneity, clustering, and local correlations that are absent in the well-mixed approximation. This quantity is not obtained by directly fitting the order-parameter curve, but from local triplet statistics measured from stationary microscopic configurations. Thus, the projected master equation should be understood as an effective Markovian description in the aggregate variable q , with transition rates informed by local network statistics. The numerical procedure for estimating $R_a(q; \epsilon)$ from stationary configurations is briefly described in Appendix A.

Using $R_a(q; \epsilon)$, the aggregate transition channels are given by $T_{+3}(q; \epsilon) = \epsilon_{\uparrow} R_0(q; \epsilon)$, $T_{+1}(q; \epsilon) = R_2(q; \epsilon)$, $T_{-1}(q; \epsilon) = R_1(q; \epsilon)$, and $T_{-3}(q; \epsilon) = \epsilon_{\downarrow} R_3(q; \epsilon)$. The mean change of q at the aggregate level is

$$\langle \Delta q \rangle_q = 3\epsilon_{\uparrow} R_0(q; \epsilon) + R_2(q; \epsilon) - R_1(q; \epsilon) - 3\epsilon_{\downarrow} R_3(q; \epsilon). \quad (5)$$

This equation shows that the aggregate drift is determined by the balance between mixed triplets, which generate ordering through majority rule, and unanimous triplets, which provide the channel for collective reversal.

For the symmetric collective-reversal case, $\epsilon_{\uparrow} = \epsilon_{\downarrow} = \epsilon$, the projected master equation for the aggregate probability $P(q, t)$ can be written as

$$\begin{aligned} \frac{dP(q, t)}{dt} = & \epsilon R_0(q-3; \epsilon) P(q-3, t) + R_1(q+1; \epsilon) P(q+1, t) \\ & + R_2(q-1; \epsilon) P(q-1, t) + \epsilon R_3(q+3; \epsilon) P(q+3, t) \\ & - [\epsilon R_0(q; \epsilon) + R_1(q; \epsilon) + R_2(q; \epsilon) + \epsilon R_3(q; \epsilon)] P(q, t). \end{aligned} \quad (6)$$

The first four terms on the right-hand side represent probability currents entering state q from states $q-3$, $q+1$, $q-1$, and $q+3$, respectively. The last term represents the probability current leaving state q . Thus, Eq. (6) is a one-dimensional master equation in the aggregate space q . Terms with indices outside the range $0 \leq q \leq N$ are discarded. The stationary distribution $P_{\text{st}}(q)$ is obtained from $dP(q, t)/dt = 0$ with the normalization $\sum_{q=0}^N P_{\text{st}}(q) = 1$.

Once the stationary distribution is obtained, the order parameter is calculated as

$$M(\epsilon) = \sum_{q=0}^N \left| \frac{2q}{N} - 1 \right| P_{\text{st}}(q), \quad (7)$$

and is compared with the MC result, $M_{\text{MC}}(\epsilon) = \langle |m| \rangle$. The absolute value is required because, in the symmetric case, the two ordered phases with positive and negative magnetization are equivalent. Therefore, $M(\epsilon)$ measures the degree of ordering without selecting either opinion direction.

With this formulation, MC simulations, the full master equation, and the projected master equation can be compared using the same observable. For small systems, the full master equation serves as an exact benchmark. For large systems, the projected master equation provides an effective reduction that still retains local information through $R_a(q; \epsilon)$.

The comparison among these three approaches is shown in Fig. 2(a). For the small system $N = 16$, the MC, full ME, and projected ME results are in very good agreement. The inset in the same panel shows that for $N = 2048$, the projected ME still follows the MC results, whereas the full ME is no longer computationally feasible because the configuration space grows as 2^N . Figure 2(b) shows the local triplet statistics R_a as a function of the positive-opinion density $c = q/N$. Solid lines show the results on the quenched network, whereas dashed lines show the annealed/mean-field prediction. The deviations between the two indicate that local

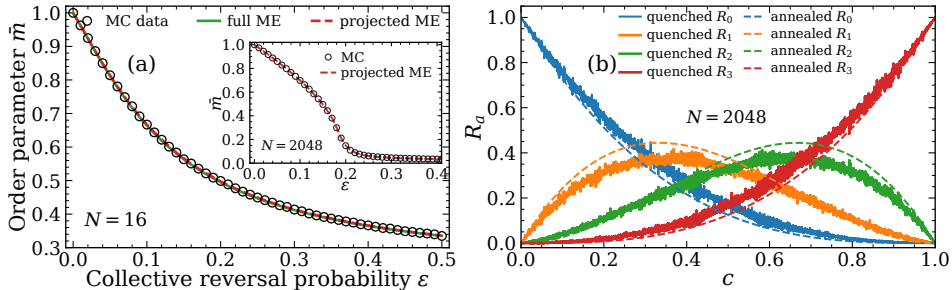


Fig. 2. Validation of the master-equation description and local triplet statistics on a BA network with attachment parameter $m_{\text{BA}} = 4$, corresponding to $\langle k \rangle \simeq 8$. (a) Order parameter $\bar{m} = \langle |m| \rangle$ as a function of the symmetric collective reversal probability ϵ for $N = 16$. The MC, full ME, and projected ME results are in very good agreement; the inset shows that the projected ME remains consistent with MC for $N = 2048$. (b) Local triplet statistics R_a as a function of $c = q/N$ for $N = 2048$. Solid lines show the quenched results, while dashed lines show the annealed/mean-field prediction. The deviations between them highlight the role of topology and local correlations in triplet statistics.

triplet frequencies are determined not only by the global density c , but also by network structure and local correlations.

The quantity $R_a(q; \epsilon)$ also provides a microscopic interpretation of the shift in the critical point. In a well-mixed population, the probability of obtaining a triplet with a positive spins follows the binomial statistics $R_a^{\text{MF}}(c) = \binom{3}{a} c^a (1-c)^{3-a}$, and therefore depends only on the global density c . On a quenched network, triplets are constrained by the local neighborhood of the central node, so $R_a(q; \epsilon)$ generally deviates from $R_a^{\text{MF}}(c)$, as shown in Fig. 2(b). This deviation changes the balance between mixed and unanimous triplets. Mixed triplets, namely $+--$ and $++-$, generate ordering through majority rule, whereas unanimous triplets, namely $---$ and $+++$, provide the collective reversal channels. Therefore, changes in the relative frequency of these two classes of triplets can shift the critical point from the well-mixed value $\epsilon_c^{\text{MF}} = 1/3$ (see Appendix B). Thus, the shift of ϵ_c on quenched networks can be understood as a direct consequence of changes in local triplet statistics, rather than merely as a finite-size effect.

3.2. Monte Carlo results and finite-size scaling

To analyze the order-disorder transition of the local triplet model on quenched networks, we first compute the order parameter, susceptibility, and Binder cumulant from MC simulations. The order parameter is defined as the mean absolute magnetization

$$M_N(\epsilon) = [\langle |m| \rangle]_{\text{dis}}, \quad m = \frac{1}{N} \sum_{i=1}^N s_i, \quad (8)$$

where $\langle \dots \rangle$ denotes a time average or MC average in the stationary state, while $[\dots]_{\text{dis}}$ denotes an average over quenched network realizations. The use of $\langle |m| \rangle$ is necessary because, in the symmetric reversal case, the two ordered states with positive and negative magnetization are equivalent. Thus, the direct average $\langle m \rangle$ may approach zero even when the system remains in an ordered phase.

Fluctuations are measured through the susceptibility χ_N , while the shape of the magnetization distribution is characterized by the Binder cumulant U_N . They are defined as^{32–34}

$$\begin{aligned}\chi_N(\epsilon) &= N \left[\langle m^2 \rangle - \langle |m| \rangle^2 \right]_{\text{dis}}, \\ U_N(\epsilon) &= \left[1 - \frac{\langle m^4 \rangle}{3 \langle m^2 \rangle^2} \right]_{\text{dis}}.\end{aligned}\quad (9)$$

The three quantities M_N , χ_N , and U_N are used together to identify the transition region and estimate the critical point. Details of the MC simulation protocol, including equilibration, number of realizations, parameter grid selection, and stationary sampling procedure, are given in Appendix A.

Figure 3 shows the MC results for BA networks with several system sizes. The BA network is generated with attachment parameter $m_{\text{BA}} = 4$, giving an average degree close to $\langle k \rangle \simeq 8$. As the symmetric collective reversal probability ϵ increases, the order parameter $\langle |m| \rangle$ decreases from a value close to one to a small value, indicating a change from the ordered phase to the disordered phase. Near the transition region, the susceptibility χ develops a peak that becomes sharper for larger system sizes. Meanwhile, the Binder cumulant curves for different N intersect around the same value, providing an initial estimate of the critical point. To improve the accuracy near the transition, the control-parameter grid is refined to $\Delta\epsilon = 10^{-3}$ around the critical region. From the crossing of the Binder cumulant curves, the best estimate for the BA network is $\epsilon_c \simeq 0.2026$. This value is smaller than the critical point of the corresponding well-mixed triplet model, $\epsilon_c = 1/3$, which can be obtained analytically or numerically.

After an initial critical point is obtained from the behavior of χ and U , we perform a finite-size scaling analysis to estimate the critical exponents. Because the system is defined on complex networks and has no characteristic linear length as in Euclidean lattices, the scaling is performed directly with the population size N . Thus, the relevant exponent is the correlation-volume exponent $\bar{\nu}$, rather than the correlation-length exponent ν .

For each network topology $\mathcal{G} \in \{\text{BA}, \text{ER}, \text{RR}, \text{WS}\}$, we assume the finite-size scaling forms^{33,34}

$$M_N^{(\mathcal{G})}(\epsilon) = N^{-\beta_{\mathcal{G}}/\bar{\nu}_{\mathcal{G}}} f_m^{(\mathcal{G})} \left[\left(\epsilon - \epsilon_c^{(\mathcal{G})} \right) N^{1/\bar{\nu}_{\mathcal{G}}} \right], \quad (10)$$

$$\chi_N^{(\mathcal{G})}(\epsilon) = N^{\gamma_{\mathcal{G}}/\bar{\nu}_{\mathcal{G}}} f_{\chi}^{(\mathcal{G})} \left[\left(\epsilon - \epsilon_c^{(\mathcal{G})} \right) N^{1/\bar{\nu}_{\mathcal{G}}} \right], \quad (11)$$

$$U_N^{(\mathcal{G})}(\epsilon) = f_U^{(\mathcal{G})} \left[\left(\epsilon - \epsilon_c^{(\mathcal{G})} \right) N^{1/\bar{\nu}_{\mathcal{G}}} \right]. \quad (12)$$

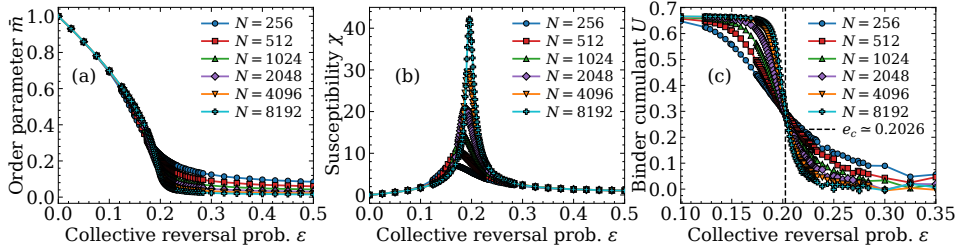


Fig. 3. Monte Carlo simulation results on BA networks with attachment parameter $m_{\text{BA}} = 4$, corresponding to $\langle k \rangle \simeq 8$. (a) Order parameter $\bar{m} = \langle |m| \rangle$, (b) susceptibility χ , and (c) Binder cumulant U as functions of the symmetric collective reversal probability ϵ for several system sizes N . The order parameter drops sharply near the transition region, while the susceptibility peak becomes more pronounced as N increases. The crossing of the Binder cumulant curves gives an estimate of the critical point $\epsilon_c \simeq 0.2026$, indicated by the vertical dashed line in panel (c). Around the critical region, each data point is obtained from up to 10^5 stationary samples and independent network realizations.

Here, $\epsilon_c^{(\mathcal{G})}$ is the critical point for topology \mathcal{G} , while $\beta_{\mathcal{G}}$, $\gamma_{\mathcal{G}}$, and $\bar{\nu}_{\mathcal{G}}$ are the critical exponents for the order parameter, susceptibility, and correlation volume, respectively.

At the critical point, Eqs. (10) and (11) yield $M_N^{(\mathcal{G})}(\epsilon_c) \sim N^{-\beta_{\mathcal{G}}/\bar{\nu}_{\mathcal{G}}}$ and $\chi_{\text{max}}^{(\mathcal{G})}(N) \sim N^{\gamma_{\mathcal{G}}/\bar{\nu}_{\mathcal{G}}}$. Therefore, the ratios $\beta_{\mathcal{G}}/\bar{\nu}_{\mathcal{G}}$ and $\gamma_{\mathcal{G}}/\bar{\nu}_{\mathcal{G}}$ are obtained from the slopes of the log-log plots of $M_N^{(\mathcal{G})}(\epsilon_c)$ and $\chi_{\text{max}}^{(\mathcal{G})}(N)$ versus N . The exponent $1/\bar{\nu}_{\mathcal{G}}$ is estimated from the shift of the pseudo-critical point. For finite systems, the susceptibility peak position $\epsilon_c^{(\mathcal{G})}(N)$ shifts from the thermodynamic critical point $\epsilon_c^{(\mathcal{G})}$ according to $|\epsilon_c^{(\mathcal{G})}(N) - \epsilon_c^{(\mathcal{G})}| \sim N^{-1/\bar{\nu}_{\mathcal{G}}}$. Thus, the slope of $\ln |\epsilon_c^{(\mathcal{G})}(N) - \epsilon_c^{(\mathcal{G})}|$ versus $\ln N$ gives $-1/\bar{\nu}_{\mathcal{G}}$. In the numerical analysis, $\epsilon_c^{(\mathcal{G})}(N)$ is determined from the position of the susceptibility peak using local interpolation around the critical region. The obtained exponents are then used in the data-collapse procedure as a consistency check.

In practice, the scaling variable is defined as $x_{\mathcal{G}} = (\epsilon - \epsilon_c^{(\mathcal{G})})N^{1/\bar{\nu}_{\mathcal{G}}}$. The values of $\epsilon_c^{(\mathcal{G})}$, $1/\bar{\nu}_{\mathcal{G}}$, $\beta_{\mathcal{G}}/\bar{\nu}_{\mathcal{G}}$, and $\gamma_{\mathcal{G}}/\bar{\nu}_{\mathcal{G}}$ are chosen so that curves for different system sizes collapse when plotted as $M_N^{(\mathcal{G})}N^{\beta_{\mathcal{G}}/\bar{\nu}_{\mathcal{G}}}$, $\chi_N^{(\mathcal{G})}N^{-\gamma_{\mathcal{G}}/\bar{\nu}_{\mathcal{G}}}$, and $U_N^{(\mathcal{G})}$ as functions of $x_{\mathcal{G}}$. A good collapse indicates that data from different system sizes are consistent with a single critical point and a single set of critical exponents for that topology. The finite-size scaling results for BA, ER, RR, and WS networks are shown in Fig. 4. In the simulations, the network parameters are chosen so that the average degree is comparable, $\langle k \rangle \simeq 8$. Specifically, BA networks are generated with attachment parameter $m_{\text{BA}} = 4$, ER networks with $p_{\text{ER}} = \langle k \rangle / (N - 1)$ and $\langle k \rangle = 8$, RR networks with fixed degree $k_{\text{RR}} = 8$, and WS networks with $k_{\text{WS}} = 8$ and rewiring probability $\beta_{\text{WS}} = 0.10$. Thus, the comparison across networks mainly highlights the effect of quenched topology, rather than a simple difference in average degree.

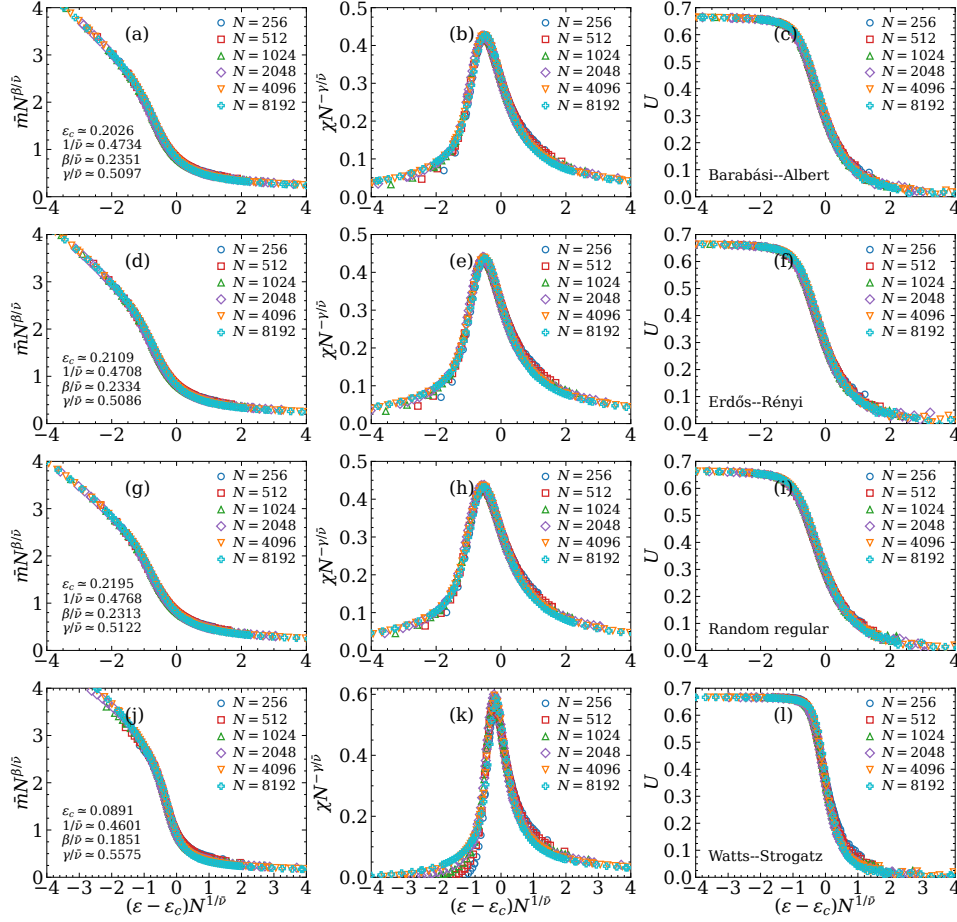


Fig. 4. Finite-size scaling collapse for the triplet dynamics on four network types: Barabási-Albert (BA), Erdős-Rényi (ER), random regular (RR), and Watts-Strogatz (WS) networks. The first to fourth rows show the results for BA, ER, RR, and WS networks, respectively. The left column shows the scaled order parameter $\bar{m}N^{\beta/\bar{\nu}}$, the middle column shows the scaled susceptibility $\chi N^{-\gamma/\bar{\nu}}$, and the right column shows the Binder cumulant U as a function of the scaling variable $(\epsilon - \epsilon_c)N^{1/\bar{\nu}}$. Different symbols denote different system sizes, from $N = 256$ to $N = 8192$. The values of ϵ_c , $1/\bar{\nu}$, $\beta/\bar{\nu}$, and $\gamma/\bar{\nu}$ used to obtain the collapse are shown in the panels of the left column.

3.3. Topology dependence and drift-based interpretation

Overall, the data for different system sizes show good collapse for each topology, with the best estimates of the critical point and critical exponents summarized in Table 1. As a reference, for the well-mixed or mean-field system, the critical point of the homogeneous triplet dynamics is $\epsilon_c^{\text{MF}} = 1/3$, with critical exponents $\beta_{\text{MF}} = 1/2$, $\gamma_{\text{MF}} = 1$, and $\bar{\nu}_{\text{MF}} = 2$. The results on quenched networks show that ϵ_c is significantly shifted from the mean-field value. For BA, ER, and RR networks, the

Table 1. Critical point and critical exponents of the triplet dynamics on different quenched networks. The mean-field/well-mixed result is shown as a reference. Numbers in parentheses indicate the estimated uncertainty in the last digit(s), obtained from variations of the fitting window, system-size range, and collapse quality.

Network	Critical point (ϵ_c)	Critical exponents		
		$\bar{\nu}$	β	γ
Mean-field / well-mixed	1/3	2	1/2	1
Barabási–Albert	0.2026(8)	2.11(5)	0.50(3)	1.08(6)
Erdős–Rényi	0.2109(9)	2.12(6)	0.50(3)	1.08(6)
Random regular	0.2195(10)	2.10(6)	0.49(3)	1.07(6)
Watts–Strogatz	0.0891(15)	2.17(8)	0.40(4)	1.21(9)

critical point lies in the range $\epsilon_c \simeq 0.20$ – 0.22 , below the well-mixed value $\epsilon_c^{\text{MF}} = 1/3$. This means that a weaker symmetric collective reversal is sufficient to destabilize the ordered phase on quenched networks. In other words, restricting interactions to local neighbors makes global order less stable than in the well-mixed system, where each agent can effectively interact with the entire population.

From a social perspective, this result suggests that consensus formed through fixed social contacts is more easily disrupted by external information than consensus in a perfectly mixed population. In real social networks, individuals usually interact only within limited environments, such as friends, communities, or work groups. As a result, local agreement formed in one part of the network may not be strong enough to sustain global order when all groups receive an external perturbation that acts symmetrically on the two opinions. Thus, a fixed social-relation structure can make collective opinion more vulnerable to external perturbations, even when the perturbation does not explicitly favor either opinion. This interpretation is consistent with recent models showing how network-induced correlations can destabilize global consensus and drive the system toward polarized states.⁴²

Interestingly, although the critical point is shifted, the critical exponents for BA, ER, and RR networks remain close to the mean-field values. The exponent β lies around 0.49–0.50, very close to $\beta_{\text{MF}} = 1/2$. Meanwhile, γ lies around 1.07–1.08, slightly larger than $\gamma_{\text{MF}} = 1$. The exponent $\bar{\nu}$ is also in the range 2.10–2.12, close to $\bar{\nu}_{\text{MF}} = 2$, although it still reflects finite-size corrections and topological effects. Therefore, BA, ER, and RR networks can be regarded as exhibiting mean-field-like critical behavior: the network topology mainly shifts the transition point, without drastically altering the critical exponents.

In contrast, the WS network exhibits more distinct behavior. Its critical point is much lower, $\epsilon_c \simeq 0.0891$, with $\beta \simeq 0.40$, $\gamma \simeq 1.21$, and $\bar{\nu} \simeq 2.17$. This deviation indicates that local correlations and the small-world structure of the WS network have a stronger influence on the collective response of the system. In other words, for the WS network, topology not only shifts the location of the transition, but also modifies the effective critical exponents more visibly than in BA, ER, and RR

networks.

To further examine this interpretation, we estimate the critical point on WS networks for several values of the rewiring probability β_{WS} using a drift-based approach built from local triplet statistics. This approach is complementary to finite-size scaling: finite-size scaling determines ϵ_c from the collective behavior of systems with several sizes N , whereas the local drift approach estimates the stability change of the fixed point $c = 1/2$ from local triplet statistics at a fixed system size.

In the symmetric collective-reversal case, the aggregate drift can be written as $F(c; \epsilon) = 3\epsilon[R_0(c; \epsilon) - R_3(c; \epsilon)] + R_2(c; \epsilon) - R_1(c; \epsilon)$. Due to up-down symmetry, the disordered state $c = 1/2$ is a fixed point. The local stability of this fixed point is determined by $\lambda(\epsilon) = \partial F(c; \epsilon)/\partial c|_{c=1/2}$, and the local critical point is estimated from the condition $\lambda(\epsilon_c) = 0$. Equivalently, by defining $R'_a(1/2; \epsilon) = \partial R_a(c; \epsilon)/\partial c|_{c=1/2}$, the local critical point can be expressed as the implicit relation

$$\epsilon_c^{\text{local}} = -\frac{R'_2(1/2; \epsilon_c) - R'_1(1/2; \epsilon_c)}{3[R'_0(1/2; \epsilon_c) - R'_3(1/2; \epsilon_c)]}. \quad (13)$$

In the numerical calculation, $R'_a(1/2; \epsilon)$ is obtained from a local fit of $R_a(c; \epsilon)$ around $c = 1/2$ using the fitting window $w = 0.06$. Since $R_a(c; \epsilon)$ is measured from stationary configurations at a given value of ϵ , Eq. (13) should be interpreted as a local stability estimate based on triplet statistics, rather than as a direct substitute for the finite-size scaling estimate.

By keeping $k_{\text{WS}} = 8$ and varying β_{WS} , this analysis separates the effect of average connectivity from that of local correlations. If ϵ_c increases as β_{WS} is increased, this indicates that the low critical point of the WS network is mainly associated with clustering and local correlations that remain strong at small rewiring probability. The results show that ϵ_c increases gradually as β_{WS} is increased, that is, as the network becomes more random, as shown in Fig. 5. It should be noted that β_{WS} is not itself a direct measure of clustering. However, in the WS construction, increasing β_{WS} systematically reduces local regularity and clustering. Therefore, the increase of ϵ_c with β_{WS} is consistent with the interpretation that strong clustering and local correlations tend to weaken the stability of the ordered phase.

For the WS network used in the finite-size scaling analysis, $\beta_{\text{WS}} = 0.10$, Table 1 gives $\epsilon_c^{\text{FSS}} \simeq 0.0891$, whereas the local drift approach in Eq. (13) gives $\epsilon_c^{\text{local}} \simeq 0.0920$, as shown in Fig. 5(a). The absolute difference between the two estimates is $|\epsilon_c^{\text{local}} - \epsilon_c^{\text{FSS}}| = 0.0029$, or about 3.26%. This difference is small and reasonable, because the two methods probe different aspects of the critical dynamics: finite-size scaling uses data from several system sizes and a collapse procedure, whereas the local drift estimate uses derivatives of triplet statistics around $c = 1/2$ for a fixed system size. Therefore, agreement within a few percent indicates that the local drift approach remains a valid microscopic diagnostic of the critical-point shift, especially for explaining the effects of rewiring, clustering, and local correlations in WS networks.

As a consistency check, the hyperscaling relation in volume form, $\bar{\nu} \simeq 2\beta + \gamma$, can

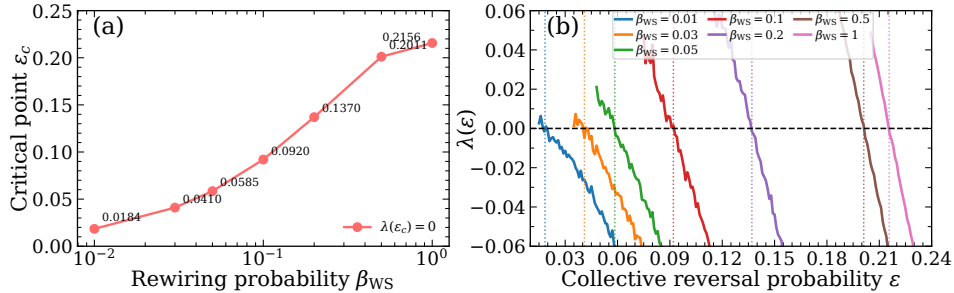


Fig. 5. Critical-point estimate on WS networks for several values of the rewiring probability β_{WS} . (a) Critical point ϵ_c as a function of β_{WS} for $N = 2048$ and $k_{WS} = 8$. The values of ϵ_c are obtained from the condition $\lambda(\epsilon_c) = 0$ and are shown near each data point. (b) Local drift $\lambda(\epsilon)$ for different values of β_{WS} , with vertical dashed lines indicating the positions of ϵ_c . For $\beta_{WS} = 0.10$, the local drift estimate gives $\epsilon_c^{\text{local}} \simeq 0.0920$, which differs by about 3.26% from the finite-size scaling estimate $\epsilon_c^{\text{FSS}} \simeq 0.0891$. The increase of ϵ_c with β_{WS} shows that the ordered phase becomes more stable as the WS network becomes more random.

also be used. For the BA network, for example, we obtain $\bar{\nu} = 2.1124$, while $2\beta + \gamma \simeq 2.0699$. The relative deviation is about 2%, indicating that the exponent estimates for the BA network are reasonably consistent with the hyperscaling relation. For ER and RR networks, the relative deviation is also only about 2–3%, whereas the WS network shows a larger deviation of about 7%. This supports the interpretation that BA, ER, and RR networks remain in a relatively mean-field-like critical regime, while the WS network exhibits stronger topological corrections.

This comparison shows that the finite-size scaling behavior of triplet dynamics on quenched networks is more topology-dependent than in the well-mixed case. For random networks with comparable average degree, such as BA, ER, and RR, the critical behavior remains in a mean-field-like regime. However, when the network has stronger local correlations, as in the WS network, the effective exponents can deviate from the mean-field values. Therefore, in addition to the symmetry of the opinion variable and the size of the state space, network topology also plays an important role in shaping the effective critical behavior of the model.

4. Summary and Conclusion

In this study, we investigated an opinion-dynamics model based on triplet majority rule with collective reversal on quenched networks. In contrast to the well-mixed model, interactions in the present model are constrained by a fixed network structure, so opinion updates take place on local triplets consisting of one central agent and two of its neighbors. Majority rule acts on mixed triplets, whereas collective reversal acts only on triplets that have reached a fully unanimous state. Thus, the model clearly separates two main mechanisms: local conformity through majority rule and external perturbations that can reverse local agreement.

To describe the aggregate dynamics on quenched networks, we used a pro-

jected master-equation formulation based on the conditional local-triplet statistics $R_a(q; \epsilon)$. This approach retains information about local network structure and correlations that are not captured by a homogeneous mean-field approximation. The validation results show that the projected master equation reproduces the MC results and, for small systems, is consistent with the full master equation. Therefore, local triplet statistics provide an effective description that connects microscopic dynamics on fixed networks with the macroscopic behavior of the system. However, since $R_a(q; \epsilon)$ is obtained from stationary microscopic configurations, this description should be understood as an effective Markovian reduction rather than a fully closed analytical theory.

Monte Carlo simulations and finite-size scaling analysis reveal a topology-dependent order–disorder transition. Compared with the well-mixed case, where the critical point is $\epsilon_c^{\text{MF}} = 1/3$, the critical point on quenched networks is shifted to lower values. For BA, ER, and RR networks, we find $\epsilon_c \simeq 0.2026$, $\epsilon_c \simeq 0.2109$, and $\epsilon_c \simeq 0.2195$, respectively, with critical exponents that remain close to the mean-field values. This indicates that, for these three networks, topology mainly shifts the location of the transition without drastically changing the class of critical behavior.

In contrast, WS networks show a more distinct response, with a much lower critical point, $\epsilon_c \simeq 0.0891$, and stronger deviations in the effective critical exponents. This indicates that clustering, local correlations, and small-world structure can weaken the stability of the ordered phase and modify the effective critical behavior. This interpretation is also supported by the local drift analysis based on triplet statistics. For the WS network with $\beta_{\text{WS}} = 0.10$, the local drift approach gives $\epsilon_c^{\text{local}} \simeq 0.0920$, differing by only about 3.3% from the finite-size scaling estimate. This agreement shows that the local drift based on $R_a(q; \epsilon)$ provides a useful microscopic diagnostic for understanding the shift of the critical point caused by network structure.

Overall, these results show that quenched network topology not only shifts the location of the transition, but also leads to topology-dependent effective critical behavior when local correlations are sufficiently strong. Local triplet statistics provide a mechanism for explaining how network structure changes the balance between ordering by majority rule and collective reversal in unanimous states. This study offers a simple framework for understanding opinion dynamics based on small-group interactions on fixed social structures. Natural extensions of this work include asymmetric collective reversal, weighted or directed networks, and networks with stronger community structure.

Acknowledgments

R. Muslim was supported by the YST Program of the Asia Pacific Center for Theoretical Physics (APCTP), funded by the Science and Technology Promotion Fund and Lottery Fund of the Korean Government, and by the Management Talent Program of the National Research and Innovation Agency of Indonesia (BRIN).

ORCIDRoni Muslim - <https://orcid.org/0000-0001-6925-5923>**Appendix A. Monte Carlo simulation protocol**

Monte Carlo simulations are performed on quenched networks using the local triplet update rule described in Sec. 2. One elementary update starts by selecting a central node r at random; if $k_r < 2$, the selection is repeated until a node with at least two neighbors is obtained. Two distinct neighbors $j, \ell \in \partial r$ are then selected uniformly at random to form the triplet $\tau = (r, j, \ell)$. Mixed triplets are updated according to the majority rule, whereas unanimous triplets may undergo collective reversal. In the main simulations, we consider the symmetric case $\epsilon_\uparrow = \epsilon_\downarrow = \epsilon$. One Monte Carlo step (MCS) is defined as N elementary updates. Four types of networks are used: BA, ER, RR, and WS, with parameters chosen so that $\langle k \rangle \simeq 8$: $m_{\text{BA}} = 4$, $\langle k \rangle = 8$ for ER, $k_{\text{RR}} = 8$, and $k_{\text{WS}} = 8$. For ER and WS networks, only connected realizations with minimum degree $k_i \geq 2$ are used.

For the finite-size scaling analysis, the system sizes are $N = 256, 512, 1024, 2048, 4096$, and 8192 . The control parameter ϵ is chosen using an adaptive grid: a coarse grid over the full range $0 \leq \epsilon \leq 0.5$, a medium grid around the critical region, and a fine grid with spacing $\Delta\epsilon = 10^{-3}$ near the critical point. The number of realizations is also adaptive, with 100, 250, and 500 realizations for the coarse, medium, and fine grids, respectively. Each run starts from a random initial condition with probability $p_{\text{init}} = 0.5$ for positive spins. Equilibration is performed adaptively with a minimum of 300 MCS and a maximum of 6000 MCS. During equilibration, block averages of $|m|$ are computed every 100 MCS; the system is considered stationary when the last three block averages differ by less than 2.0×10^{-3} . After equilibration, measurements are performed for 4000 MCS, and configurations are sampled every 20 MCS. From the stationary magnetization series, M_N , χ_N , and U_N are computed as defined in Sec. 3.

For the validation of the projected master equation, the conditional triplet statistics $R_a(q; \epsilon)$ are estimated from stationary MC configurations. For each measured configuration, the value of q is recorded, and local triplets are sampled using the same selection rule as in the dynamics. The fraction of triplets with $a = 0, 1, 2, 3$ positive spins is then averaged over all configurations with the same value of q and over network realizations. In the comparison between MC and the projected ME for $N = 2048$, we use 500 realizations for each value of ϵ , 4000 MCS for measurement, sampling every 20 MCS, and 2000 sampled triplets per configuration. Thus, each value of ϵ provides $500 \times (4000/20) = 10^5$ stationary configurations for estimating the triplet statistics. For small systems, the MC and projected ME results are also compared with the full master equation.

For the drift-based estimate of the critical point on WS networks, we use $N = 2048$, $k_{\text{WS}} = 8$, and several values of the rewiring probability β_{WS} . For each β_{WS} , the parameter ϵ is taken on a local grid with spacing $\Delta\epsilon = 10^{-3}$ around the critical

region. The triplet statistics $R_a(c; \epsilon)$ are computed from stationary configurations, and the derivatives $R'_a(1/2; \epsilon)$ are obtained from a weighted linear fit in the window $|c - 1/2| \leq 0.06$. The local drift is defined as $F(c; \epsilon) = 3\epsilon[R_0(c; \epsilon) - R_3(c; \epsilon)] + R_2(c; \epsilon) - R_1(c; \epsilon)$, while the stability of the disordered state is determined by $\lambda(\epsilon) = \partial F / \partial c|_{c=1/2}$. The local critical point is obtained from the condition $\lambda(\epsilon_c) = 0$, using linear interpolation between two consecutive values of ϵ where λ changes sign.

Appendix B. Critical point in the annealed limit

In the annealed or well-mixed limit, triplets are selected randomly from the entire population. If c is the density of agents with opinion $+1$, the probability of selecting a triplet with a positive spins follows the binomial distribution $R_a^{\text{MF}}(c) = \binom{3}{a} c^a (1-c)^{3-a}$, with $a = 0, 1, 2, 3$. For the symmetric collective-reversal case, $\epsilon_\uparrow = \epsilon_\downarrow = \epsilon$, the mean-field drift is $F_{\text{MF}}(c; \epsilon) = 3\epsilon[R_0^{\text{MF}}(c) - R_3^{\text{MF}}(c)] + R_2^{\text{MF}}(c) - R_1^{\text{MF}}(c)$. Substituting the binomial form gives

$$F_{\text{MF}}(c; \epsilon) = 3(2c - 1) [c(1 - c) - \epsilon(1 - c + c^2)]. \quad (\text{B.1})$$

Due to up-down symmetry, $c = 1/2$ is always a fixed point. Its local stability is determined by $\lambda_{\text{MF}}(\epsilon) = \partial F_{\text{MF}} / \partial c|_{c=1/2} = \frac{3}{2}(1 - 3\epsilon)$. The critical point is obtained from $\lambda_{\text{MF}}(\epsilon_c) = 0$, yielding $\epsilon_c^{\text{MF}} = 1/3$.

References

1. P. Clifford and A. Sudbury, *Biometrika* **60**, 581 (1973).
2. R. A. Holley and T. M. Liggett, *Ann. Probab.* **3**, 643 (1975).
3. S. Galam, *Int. J. Mod. Phys. C* **19**, 409 (2008).
4. C. Castellano, S. Fortunato and V. Loreto, *Rev. Mod. Phys.* **81**, 591 (2009).
5. A. Sirbu, V. Loreto, V. D. Servidio and F. Tria, Opinion dynamics: models, extensions and external effects, in *Participatory sensing, opinions and collective awareness*, (Springer, 2016), pp. 363–401.
6. H. Noorazar, K. R. Vixie, A. Talebanpour and Y. Hu, *nt. J. Mod. Phys. C*. **31**, p. 2050101 (2020).
7. H. Noorazar, *Eur. Phys. J. Plus.* **135**, p. 521 (2020).
8. A. F. Peralta, J. Kertész and G. Iñiguez, Opinion dynamics in social networks: From models to data, in *Handbook of Computational Social Science*, (Edward Elgar Publishing Limited, 2025), pp. 384–406.
9. A. Flache, M. Mäs, T. Feliciani, E. Chattoe-Brown *et al.*, *J. Artif. Soc. Soc. Simul.* **20** (2017).
10. S. Galam, *Eur. Phys. J. B.* **25**, 403 (2002).
11. P. L. Krapivsky and S. Redner, *Phys. Rev. Lett.* **90**, p. 238701 (2003).
12. P. Chen and S. Redner, *Phys. Rev. E* **71**, p. 036101 (2005).
13. C. Castellano, M. A. Muñoz and R. Pastor-Satorras, *Phys. Rev. E*. **80**, p. 041129 (2009).
14. P. Nyczka, K. Sznajd-Weron and J. Cisko, *Phys. Rev. E* **86**, p. 011105 (2012).
15. W. Radosz, A. Mielnik-Pyszcorski, M. Brzezińska and K. Sznajd-Weron, *Phys. Rev. E* **95**, p. 062302 (2017).
16. A.-L. Barabási and R. Albert, *Science* **286**, 509 (1999).

18 R. Muslim

17. D. J. Watts and S. H. Strogatz, *Nature* **393**, 440 (1998).
18. L. F. Pereira and F. B. Moreira, *Phys. Rev. E* **71**, p. 016123 (2005).
19. F. Lima, *Commun. Comput. Phys.* **2**, 358 (2007).
20. A. Jedrzejewski, *Phys. Rev. E* **95**, p. 012307 (2017).
21. A. Jedrzejewski and K. Sznajd-Weron, *Phys. Rev. E* **105**, p. 064306 (2022).
22. D. Alencar, J. S. Neto, T. Alves, F. Lima *et al.*, *Phys. Rev. E* **110**, p. 044306 (2024).
23. D. A. Mulya and R. Muslim, *Int. J. Mod. Phys. C* **35**, p. 2450125 (2024).
24. M. Cinelli, G. De Francisci Morales, A. Galeazzi, W. Quattrociocchi and M. Starnini, *PNAS* **118**, p. e2023301118 (2021).
25. P. Nyczka and K. Sznajd-Weron, *J. Stat. Phys.* **151**, 174 (2013).
26. J. Civitarese, *Phys. Rev. E* **103**, p. 012303 (2021).
27. A. Abramiuk and K. Sznajd-Weron, *Entropy* **22**, p. 120 (2020).
28. M. Mobilia, *Physics* **5**, 517 (2023).
29. Azhari and R. Muslim, *Int. J. Mod. Phys. C* **34**, p. 2350088 (2023).
30. R. Muslim, D. A. Mulya, Z. Akbar and R. A. Nqz, *Chaos Soliton Fract.* **189**, p. 115718 (2024).
31. P. Mullick and P. Sen, *PLoS One* **20**, p. e0316889 (2025).
32. K. Binder, *Z. Phys. B: Condens. Matter.* **43**, 119 (1981).
33. V. Privman, *Finite size scaling and numerical simulation of statistical systems* (World Scientific, 1990).
34. D. Landau and K. Binder, *A guide to Monte Carlo simulations in statistical physics* (Cambridge university press, 2021).
35. B. J. Zubillaga, A. L. Vilela, M. Wang, R. Du, G. Dong and H. E. Stanley, *Sci. Rep.* **12**, p. 282 (2022).
36. H. Schawe and L. Hernández, *Commun. Phys.* **5**, p. 32 (2022).
37. N. Papanikolaou, R. Lambiotte and G. Vaccario, *Physica A* **630**, p. 129257 (2023).
38. I. Iacopini, M. Karsai and A. Barrat, *Nat. Commun.* **15**, p. 7391 (2024).
39. J. Kim, D.-S. Lee, B. Min, M. A. Porter, M. San Miguel and K.-I. Goh, *Phys. Rev. E* **111**, p. L052301 (2025).
40. R. Muslim, J.-M. Park, J. Kim and R. A. NQZ, *arXiv preprint arXiv:2602.01902* (2026).
41. F. Battiston, G. Cencetti, I. Iacopini, V. Latora *et al.*, *Phys. Rep.* **874**, 1 (2020).
42. F. Baumann, P. Lorenz-Spreen, I. M. Sokolov and M. Starnini, *Phys. Rev. Lett.* **124**, p. 048301 (2020).